# Elderly Bodily Assistance Robot (E-BAR): A Robot System for Body-Weight Support, Ambulation Assistance, and Fall Catching, Without the Use of a Harness

Roberto Bolli Jr. and H. Harry Asada[1]

***Abstract*— As over 11,000 people turn 65 each day in the U.S., our country, like many others, is facing growing challenges in caring for elderly persons, further exacerbated by a major shortfall of care workers. To address this, we introduce an eldercare robot (E-BAR) capable of lifting a human body, assisting with postural changes/ambulation, and catching a user during a fall, all without the use of any wearable device or harness. Our robot is the first to integrate these 3 tasks, and is capable of lifting the full weight of a human outside of the robot's base of support (across gaps and obstacles). In developing E-BAR, we interviewed nurses and care professionals and conducted user-experience tests with elderly persons. Based on their functional requirements, the design parameters were optimized using a computational model and trade-off analysis. We developed a novel 18-bar linkage to lift a person from a floor to a standing position along a natural trajectory, while providing maximal mechanical advantage at key points. An omnidirectional, non-holonomic drive base, in which the wheels could be oriented to passively maximize floor grip, enabled the robot to resist lateral forces without active compensation. With a minimum width of 38 cm, the robot's small footprint allowed it to navigate the typical home environment. Four airbags were used to catch and stabilize a user during a fall in $\leq$ 250 ms. We demonstrate E-BAR's utility in multiple typical home scenarios, including getting into/out of a bathtub, bending to reach for objects, sit-to-stand transitions, and ambulation.**

***Index Terms*— Physically Assistive Devices, Domestic Robotics, Mechanism Design of Mobile Robots.**

## I. Introduction

The challenge of caring for elderly persons has emerged as a significant societal issue, driven by demographic shifts, evolving family structures, and the rising cost of healthcare. According to the UN, the global population aged 65 and older is expected to increase to 1.6 billion by 2050 [1], representing 16% of the total population - the highest ever in human history. Changes such as increased geographic mobility and smaller family sizes are contributing to a shift in caregiving responsibilities away from relatives and towards hired labor. However, the cost of eldercare services such as nursing homes has remained persistently high in recent years, with a median cost of $108,405/year in the United States [2]. There is also a shortage of caregivers in the U.S. workforce, with vacancy rates ranging from 20 to 25 percent [3], and this is expected to worsen in the coming decades.

Compounding these issues, 92% of elderly persons express a strong preference to age in their homes [4]. This often leads to situations where they are unable to perform desired tasks, such as bending down to retrieve an item from the floor, or perform such tasks safely without falling, due to age-related imbalance, weakened muscles, or syncope. Falls are particularly common among older adults: nearly 14 million (1 in 4) fall each year in the U.S. alone, and falls are the leading cause of injury for people aged 65 and older [5]. Fall-related injuries hasten the progression to long-term care facilities and nursing homes, and a portion even lead to death.

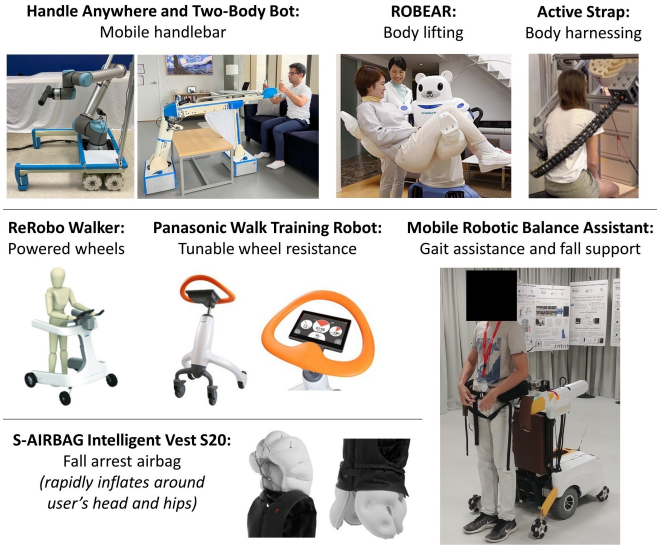


Fig. 1. Examples of eldercare robots, classified by function. From top to bottom row, left to right: body-weight support and/or human body lifting [6] [7] [8] [9], active walkers [10] [11], and fall mitigation [12] [13]. Note that the Mobile Robotic Balance Assistant is able to provide both gait assistance and fall catching, with the caveat of requiring the user to wear a harness.

Accordingly, multiple robots have been developed to augment or replace the physical assistance provided by human caretakers. Representative examples of such devices are shown in Fig. 1 (ref. [6] - [13]), classified by function. Besides reducing the need for human labor, these robots present several advantages compared to conventional solutions such as grab bars, canes, and walkers. The specific advantages depend on the robot system, but in general, mobile robots allow for body support to be placed at a biomechanically optimal location for a specific postural transition. It is often infeasible to place assistive devices such as grab bars at these locations due to room geometric constraints. Furthermore, a mobile robot can move out of the way after the user performs a movement, allowing for other movements to

[1]Roberto Bolli Jr. and H. Harry Asada are with the Department of Mechanical Engineering at the Massachusetts Institute of Technology, 77 Massachusetts Ave., Cambridge, MA, USA. rbolli, asada@mit.edu

proceed unobstructed. Navigation capabilities, balance, and the muscle function of the user can also be augmented by robotic systems, delaying the transition to nursing homes and allowing for safe aging-in-place.

While these robots have yielded promising results, their utility has generally been limited to specific tasks. For a robot to be truly functional in a home setting, supporting the user in everyday life, it should be able to perform all of the functions in Fig. 1: body-weight support/lifting, gait assistance, and fall mitigation/catching. Although various assistive devices are available for each of these tasks, it is not practical and even dangerous for older adults to change equipment on their own [14]. We are not aware of any single eldercare robot that can accomplish all of these tasks seamlessly, especially without the use of a harness. The latter is particularly important because elderly persons overwhelmingly do not like to wear harnesses or other devices that limit freedom of movement [15], and in most cases, another person is required to put the device on the user. Robots that provide bodily support additionally tend to be large and bulky, making navigation of the home environment difficult.

Therefore, we have set out to create a mobile robot designed specifically for aging in place at home, or assisting caregivers at a care facility, without the use of a harness. Our goal is for the robot to function as a non-visible safety net (located behind the user) with a compact footprint, providing both body support and fall catching when necessary. Based on discussions with caregivers, we targeted the subgroup of elderly persons who retain significant or medium muscle strength, but require assistive devices for activities of daily living. This comprises 24% of U.S. adults aged 65 and older, and the percentage increases with age [16]. Overlapping with this group are persons with balance deficiencies; around 28% of U.S. adults over 75 are indicated for increased fall risk in clinical assessments such as the 4-Stage Balance Test [17]. Together, these groups represent a large portion of the elderly population that is underserved by current care systems.

To inform the design and functionality of the robot, we consulted with multiple elderly persons, caregivers, and medical professionals. We discuss their input, as well as our design process, in section 2. Section 3 introduces a novel 1-DoF linkage we have developed for body-weight support across a wide height range. In section 4, we present the robot's high-friction, nonholonomic, omnidirectional drive base and the associated control scheme. Section 5 focuses on the design of the airbags to catch a user during a fall. Section 6 demonstrates the robot's utility in a variety of challenging settings, with input from elderly persons and caregivers, as a proof-of-concept. We offer a brief conclusion and discussion of future work in section 7.

## II. Robot Design

We employed a user-centered development process, incorporating feedback from care professionals and elderly persons at various points along the project timeline (Fig. 2). Based on our goal of supporting diverse tasks in a home

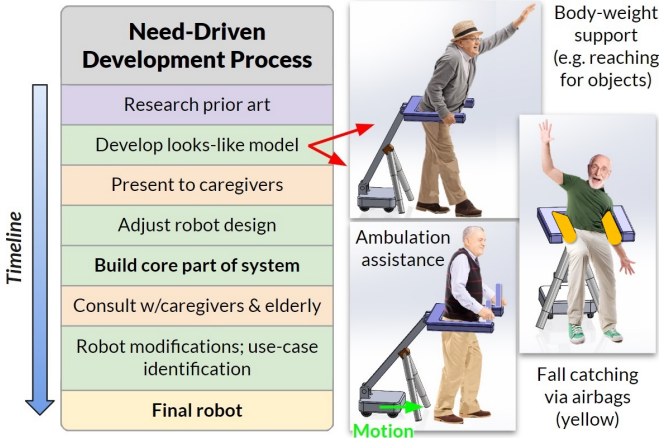


Fig. 2. The user-centered development process employed while building the E-BAR robot. Green cells represent building and design work, while orange cells show instances where user/caregiver feedback was sought. The looks-like model consists of a small-footprint omnidirectional drive base (gray), enabling the user to move in any direction, attached to a height-adjustable u-shaped fork (blue). The fork a) adds stability via lateral bracing, b) provides a surround structure for the user to hold or grab onto while facing any direction, c) allows unobstructed entry and exit, and d) can lift a user from their armpits or forearms (when placed on the sides of the fork).

setting with a single assistive system, a core set of **functional requirements** were defined:

1) Footprint of less than 64 cm x 64 cm to fit through the minimum doorway width of 70 cm in Massachusetts [18] and navigate around obstacles.
2) Open area around the user's legs, equal to at least a half stride, for unobstructed movement.
3) Able to support the full weight of an ∼80 kg user:
   a) >120 N lateral load bearing [19].
   b) 800 N vertical load bearing.
4) Translation along any direction (omnidirectional), to avoid impeding the user's natural movements.

From these, we developed a looks-like model (described in Fig. 2), which was presented to approximately a dozen caregivers and medical professionals. Overall, they were supportive of the proposed device, calling it a much-needed assistive tool and mentioning it could also increase patient functionality as a form of physical therapy. Common points raised during the feedback session became additional functional requirements for the robot:

5) Airbags must inflate rapidly and exert a strong grip, since elderly persons are frequently unable to arrest a fall using their own muscle strength.
6) Robot physically interacts with the user safely, providing forearm support, with no risk of tipping or slipping.
7) Does not require the user to wear specific clothing.

### A. Computational Optimization of Design Parameters

Based on an initial needs assessment and the core functional requirements above, a basic design was developed, expanding on the looks-like model in Fig. 2. This consisted of a heavy, omnidirectional drive base attached to a u-shaped fork via a powered linkage. A pair of ball casters were added to prevent the robot from tipping forwards. The design was

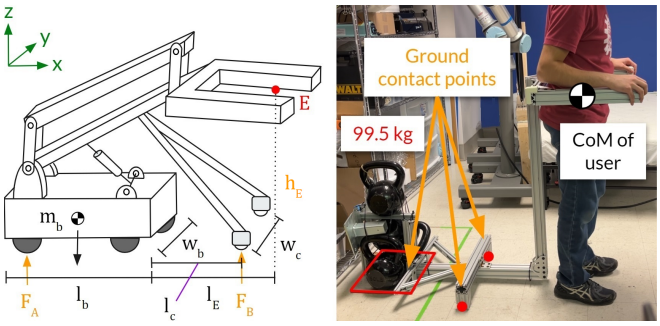


Fig. 3. Left: robot design parameters that were optimized via a cost function. $l_b$, $w_b$ and $m_b$ are the length, width, and mass of the base; $l_c$ is the distance from the base to the casters, $w_c$ is the spacing between the casters, and $l_E$ is the ground distance from the base to the user. $h_E$ is the height from the ground to the user's CoM (E). Right: experimental validation of the optimization output via a works-like model of the robot structure.

TABLE I

COMPUTATIONAL OPTIMIZATION CONSTRAINTS

| Constraint | Justification |
|---|---|
| $29.5 \text{ kg} \leq m_b \leq 100 \text{ kg}$ | Home floors can safely support up to a 180 kg point load [20]. Over 100 kg could lead to damage of the robot's drivetrain. |
| $25.4 \text{ cm} \leq l_b, w_b, w_c \leq 64 \text{ cm}$ | The robot must occupy a small footprint. |
| $l_c = l_E - 35.6 \text{ cm}$ | Prevents the front ball casters from interfering with the user's motions. |
| $53.3 \text{ cm} \leq l_E \leq 88.9 \text{ cm}$ | An older adult's stride length is around 75 cm [21], and the robot base must be at least half a step away from the user. |
| $h_E = 99 \text{ cm}$ | Approximate height of the center of mass of the average US male [22]. |
| $F_A, F_B > 0$ | Ground contact forces must be positive or the robot will tip over. |
| $\mu F_A + \mu F_B - F_x \geq 0$<br>$\mu F_A + \mu F_B - F_y \geq 0$ | Static force balance with frictional anti-slip force. From functional requirements, max. lateral force is $F_x = F_y = 120$ N. |
| $M_x - \frac{m_b g w_c}{2} \leq 0$ | Static moment balance to prevent tipping. $M_x = -h_E F_y - (\text{fork width})/(2F_z)$. To accommodate the maximum expected user girth, the fork width was set to 50 cm. |

decomposed into key parameters (Fig. 3, left) that determined the overall shape, weight, and form of the robot. As opposed to manually selecting the value of each parameter, such as through trial and error, an optimal combination was obtained by minimizing a cost function. This design methodology maximized performance while allowing us to quantify the relative importance of parameters in conflict with each other (e.g. how much to value narrow width over lighter weight).

To ensure that the robot design satisfied the functional requirements, the parameters were subjected to the constraints in Table 1. The static ground friction was set at $\mu = 0.5$, which is expected for common home surfaces [7]. We then defined a cost function $V$ to minimize:

$$V = c_0 m_b^* + c_1 l_b^* + c_2 w_b^* - c_3 l_E^* + c_4 l_c^* + c_5 w_c^* \quad (1)$$

where $c_0 \ldots c_6$ are weights specified by the designer. Negative signs reflected parameters we wished to maximize instead of minimize. To avoid biasing the cost function towards parameters with a large dynamic range, each parameter $p$ was normalized to $[0, 1]$ via the following:

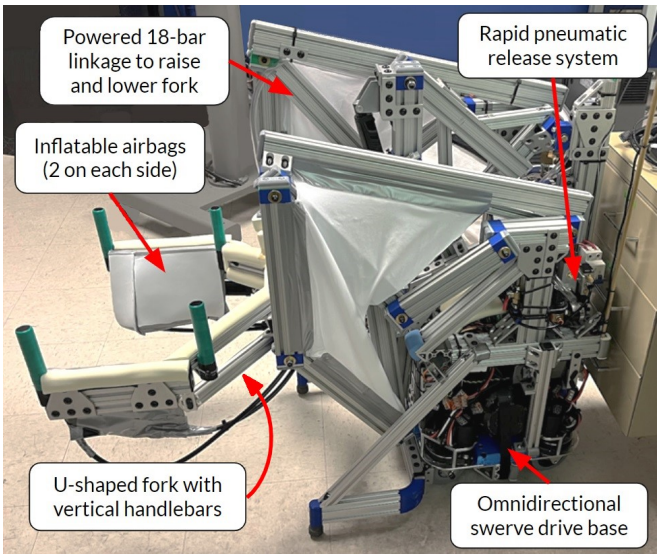


Fig. 4. The E-BAR robot system. For high traction, each wheel module is capable of independent rotation and translation. Airbags on the fork inflate rapidly during a fall, catching the user via friction and contact pressure.

$$p^* = \frac{p - p_{min}}{p_{max} - p_{min}} \quad (2)$$

where $p_{max}$ and $p_{min}$ are the extrema of the acceptable range of values for the parameter, specified in Table 1.

A Monte Carlo simulation was used to generate over 1 billion combinations of the 6 parameters, with each parameter sampled from a uniform distribution across its specified range. This ensured the result reflected the global optimum instead of a local optimum. Each parameter combination was checked against the constraints to assess compliance. $c_0 \ldots c_3$ and $c_5$ were set to 1, while $c_4$ was set to 1.5 to bringing the front ball casters close to the drive base, reflecting our high value on making the robot compact.

The results were validated by testing the load-bearing capacity and lateral force resistance on a works-like model of the robot (Fig. 3, right), whose design parameters were equal to the output of the simulation. Adult test subjects ($\leq 80$ kg) were not able to tip the model or cause it to slip laterally by leaning on the inside of the fork. The optimization relaxed the inherent conflicts between functional requirements 1, 2, and 3 by employing a large base mass ($m_b = 99.5$ kg) and adjusting the ball caster locations ($l_c = 30$ cm, $w_c = 51$ cm) to make the drive base more compact ($l_b = w_b = 25.6$ cm) with a long maximum reach of $l_E - l_c = 58$ cm. This stands in contrast to most existing eldercare robots, which require the user to be within the base of support (i.e. $l_E - l_c \leq 0$). The design parameters were further modified for the final system to address practical limitations in implementation.

### B. Final Robot System

Additional interviews with care professionals led to concerns that accidental collisions with the robot may lead to injury, as the skin of elderly persons is easily bruised. Accordingly, sharp points on the robot were padded with gray foam, and any potential pinch points were covered. The

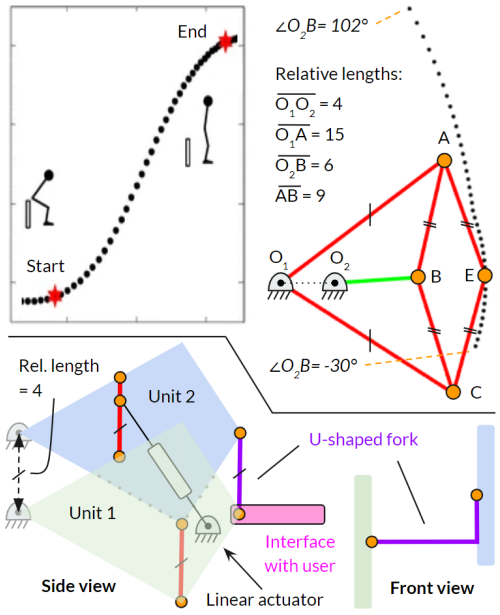


Fig. 5. Top left: typical sit-to-stand trajectory of the CoM of an adult, adapted from [26]. The spacing between dots indicates the speed of the movement. Top right: the core functional unit of the linkage, with the corresponding endpoint path when link $O_2B$ (green) traverses its range of motion at a constant speed. Bottom: abstraction of the full 18-bar linkage structure, comprised of two functional units connected in parallel by redundant links. A linear actuator drives the system. The part of the u-shaped fork interfacing with the user (pink) remains parallel to the ground.

final system is shown in Fig. 4. The fork was also padded to reduce pressure on the forearms while lifting the user, and augmented with four handlebars to allow the user to grip the fork while facing both towards and away from the robot.

The robot's ground footprint formed a compact trapezoid with a rear width of 38.1 cm, front width of 48.9 cm, and perpendicular length of 63.5 cm. Base mass $m_b$ was increased to 110 kg to add a factor of safety, further minimizing the possibility of the robot tipping even under extreme loads. The front of the u-shaped fork could extend up to 46 cm from the ball casters, allowing the robot to span a wide obstacle such as a bathtub lip. All aspects of the design satisfied the functional requirements listed previously.

## III. Linkage for Raising the Fork

When lifting a person's body, the u-shaped fork should traverse a trajectory emulating natural human movement, while the robot base remains stationary for high traction. This requires the fork to translate both vertically and towards/away from the user. In addition, the output force and velocity should complement the user's muscle action, and the linkage geometry should not obstruct any limb or trunk motion. This excludes any linkage configuration with pivots or ground-link attachment points placed above, below, or in front of the user.

We begin by defining the necessary range of motion. The fork should be able to lift between 46 cm and 137 cm high, which roughly corresponds to the armpit height of the average U.S. male while seated on the floor and standing, respectively [22]. This allows the fork to sit underneath

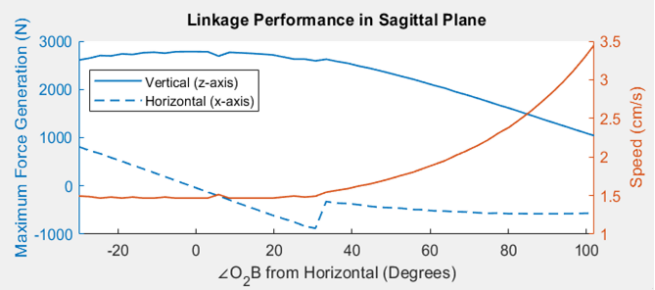


Fig. 6. Load bearing and speed curves of the linkage endpoint (u-shaped fork). Matlab was used to numerically simulate the linkage kinematics, determining the lossless power transmission from the driving link to the endpoint. The 3000 N max, 1 cm/s (at lower load) linear actuator was converted to an equivalent constant angular velocity and torque, driving link $O_2B$. Since the actual angular velocity of $O_2B$ increases as the linear actuator fully extends, the roll-off of both the speed and vertical force generation curves ($\angle O_2B > 80°$) is steeper than in the plot.

the arms of the user, providing physical support for most biomechanically feasible motions. Previous linkages have been designed for specific motions such as sit-to-stand [23] [24], but to maintain the generalized functionality of the robot for lifting and support across a wide range of body poses, we consider the **hybrid of two trajectories: squat-to-stand and sit-to-stand**, which are merged to create the lower and upper parts of the linkage path, respectively. A squat-to-stand trajectory is approximately vertical [25], with some tolerance for horizontal motion. This contrasts with a typical sit-to-stand trajectory (Fig. 5, top left), which curves forwards. As a trade-off between number of links (increased mechanical complexity) and path fidelity, 8 bars were used to approximate the desired fork path (Fig. 5, top right).

The weight offloaded to the fork will be approximately constant at the lower and middle parts of the linkage path, whether the user is being lifted directly or is assisting using their legs. This is because leg muscles generate a roughly constant force at the CoM during the lower phase of a sit-to-stand transition, resulting in a linearly increasing CoM velocity [27]. Therefore, the mechanical advantage of the linkage should also be constant along this part of the linkage path. In postures closer to a standing position, a person is capable of faster motions, and more weight is offloaded to the legs. Therefore, the mechanical advantage should decrease (so the speed will increase) as the linkage approaches its upper limit. Our linkage displays these trends in Fig. 6.

### A. Kinematic Structure

The core functional unit (Fig. 5, top right) is based on a modification of the Peaucellier–Lipkin inversor, which converts rotary motion to linear motion. By carefully choosing the link lengths, as driving link $O_2B$ rotates, the rhombus $ABCE$ compresses to extend the endpoint $E$ away from point $B$ and along our desired trajectory. Lengthening the gap between $O_1$ and $O_2$ causes the path to become more linear; shortening this distance causes the endpoint to curve inwards near the top and bottom of the path. We use a specific asymmetric range for the driving link ($-30°$ to $102°$) to capture the approximately straight trajectory when $E$ is

near $O_2$ and curving trajectory when it is far away.

To keep the fork parallel to the ground, two functional units (blue and green in Fig. 5, bottom left) are separated by a vertical gap (black dashed arrow), and connected by three congruent links (red and purple) with the same length as the gap. This causes the fork link (purple) to act as a parallel motion 4-bar linkage with the vertical gap, which keeps the fork body (pink) parallel to the floor. The functional units are also separated by a horizontal distance (Fig. 5, "Front view") to better support imbalanced loads caused by weight on one side of the fork. A redundant link between the bottom of unit 1 and unit 2 prevents the top link from getting stuck in a singularity when it crosses vertically over $O_1$. As the rhombus $ABCE$ of each functional unit allows for minor movement along the line extending from $B$ to $E$, the fork link (purple) does not overconstrain the other parallel links (red), and distributes the load on the fork to both functional units.

A non-backdrivable linear actuator is used to drive the 18-bar, 1-DoF system (Fig. 5, bottom left), which allows for a high lifting force of over 2700 N (Fig. 6) and automatic locking at any point along the path. The linkage can be fully raised in approximately 45 seconds. It meets all of the load-bearing and lateral force requirements listed in section 2.

## IV. Drive Base and Control Scheme

The drive base consists of four modules (MK4, Swerve Drive Specialties) with 10 cm diameter wheels, arranged along the vertices of a 25.4 cm square, as shown in Fig. 7. Each wheel was equipped with a high-traction thermo-plastic elastomer tread (65 Shore A hardness), resulting in a coefficient of friction $\mu_s$ = 0.8-1.2 on hard flooring and low-pile carpet [28]. The velocity and orientation of each wheel could be controlled independently for omnidirectional, nonholonomic movement. This contrasts with active casters [29], which have a gap between the longitudinal axis of rotation and ground contact point to achieve holonomicity. However, the lack of a gap (Fig. 7, left) results in passive traction perpendicular to the wheel plane, which provides inherent resistance orthogonal to the wheel's direction of motion. We leverage this property by parking the robot in an x-shaped wheel configuration that maximizes traction (Fig. 7, right). External torque results in motion completely orthogonal to each wheel, and external $x$ and $y$ forces result in motion at a 45° angle to each wheel, distributing the wheel traction equally along the $x$ and $y$ axes. In experimental tests, the user could exert over 265 N (x-axis) and 155 N (y-axis) on the base of the fork before the wheels began to slip, exceeding our functional requirements.

The orientation of each wheel was maintained through proportional feedback control, with steering torque limited to $\leq$ 5 N·m to avoid instability. A 3-axis joystick was used for manual control of the robot system at up to 0.5 m/s, capped for safety. The vector created by tilting the joystick along its longitudinal axes was mapped to a target wheel orientation and velocity (Fig. 7, green), causing the base to translate. Twisting the joystick past a threshold switched the wheels to a radially symmetric configuration (Fig. 7, purple), rotating the base at a speed proportional to the applied twist. This scheme was chosen due to its ease of use by elderly persons and robustness in navigation; all operators learned to drive the robot in a couple of minutes.

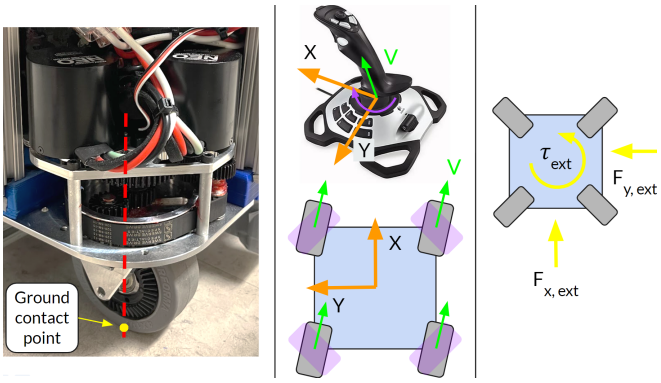


Fig. 7. Left: swerve drive module for independent control of wheel velocity and orientation. An absolute encoder measures rotation about the steering axis (red). Middle: joystick tilt $\vec{v}$ is mapped to wheel pose and velocity to translate the base in the $xy$ plane. Twisting the joystick switches the wheels to the configuration shown in purple, causing pure rotation. Right: x-shaped wheel configuration for maximum resistance to external torques and forces.

## V. Air Bags for Fall Catching

When an elderly person falls, it takes on average 688 ms between the imbalance onset and start of descent [30], and a fall can be reliably predicted around 250 ms before the descent occurs [31]. Accordingly, the airbags must fully inflate and catch the user's pelvis within 250 ms. In addition, the airbags must have sufficient friction with the user's clothes to hold the user without slippage, but the pressure must be distributed along a large area of skin to prevent bruising. We found that the limiting factor is friction between the user's skin and clothes, since certain foams (used on the airbags' outer covers) have very high friction with clothing. Bruising typically occurs when skin pressure exceeds 3.9 MPa [32], and is lower in elderly persons. Under quasi-static assumptions and a low clothes-to-skin friction of $\mu_s = 0.51$ (woven cotton, see [33]), a contact area $A$ of 110 cm$^2$ on each side (total area $2A$) is necessary to catch an 80 kg person with a conservative airbag pressure $P$ of 0.07 MPa, providing a safety factor of 50 against skin bruising.

$$\sum F_z = mg - 2AP\mu_s = 0 \tag{3}$$

To prevent the user from falling forwards, a trapezoidal airbag configuration was employed on each side, consisting of a large airbag (Fig. 8, top left, A) for contacting the body and a smaller airbag to constrain forward motion (B). All four airbags were constructed from 0.15 mm thick poly tubing, heat sealed at both ends to form a chamber, and attached to the fork at the top edge. It was found that wrapping the chambers with duct tape for reinforcement prevented tears caused by turbulent flow during the rapid inflation phase. User-facing surfaces were covered with 0.64 cm thick neoprene closed-cell foam to effectively grip clothing. The airbag size accommodated users with a pelvis width of up

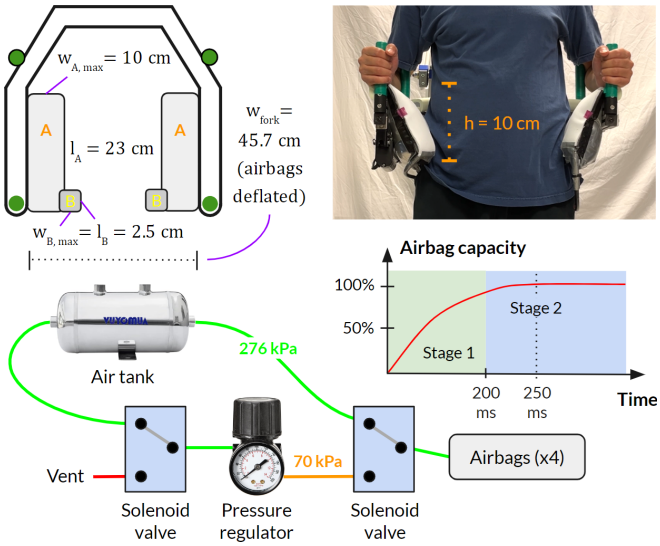


Fig. 8. Top left: airbag placement on the robot's u-shaped fork. The airbags were flat when not in use. Top right: pressurized airbags gripping the user's CoM, with a large contact area on each side ($\geq$110 cm$^2$). Bottom: schematic of the rapid air fill system, along with a representational graph of the filling process. In stage 1, the airbags are quickly inflated to 80-90% capacity, while in stage 2, inflation finishes and pressure is maintained at 70 kPa.

Fig. 9. Six of multiple possible assistance scenarios. Top row: getting into/out of a bathtub, bending down to reach objects, and catching a fall. Bottom row: powered sit-to-stand transition from a toilet, lifting a person from the floor, and walking assistance. Due to IRB restrictions, tasks involving higher risk were tested with an adult.

to 40 cm, ensuring that in any direction any user was facing, the inflated contact area was likely to be $\geq$ 110 cm$^2$.

A 2-stage pneumatic fast-fill system was devised to inflate the airbags rapidly (Fig. 8, bottom). In the first stage, a direct connection to an air tank pressurized at 276 kPa was opened for a period of 200 ms, filling the airbags to 80-90% capacity. The airflow was then switched to a 70 kPa pressure-regulated stream that inflated the airbags to 100% capacity within 50 ms and maintained the air pressure against small leaks. Compared to alternative inflation systems, ours did not require active pressure measurement or holes in the airbags to vent excess pressure, and allowed for the use of low-cost, low-precision solenoid valves (Tailonz 4V210, 4V410).

## VI. Use Case Studies

We consulted with three caregivers and four elderly persons who could benefit from postural assistance to find activities of daily living that the robot could best support, as well as potential modes of assistance (e.g. whether the robot would be useful as a walker). Based on their feedback, the six scenarios shown in Fig. 9 were tested as a proof-of-concept, with the users able to control the robot and trigger the airbags via a wireless joystick. Caregivers indicated that the magnitude of assistance should depend on the functional level of the person, with high-level walking support reserved only for those with the best mobility. Accordingly, for some tasks (e.g. bending down), the robot's fork was used a structure to lean or grab onto, while for others, the robot provided active assistance by lifting the fork (e.g. entering/exiting a bathtub, sit-to-stand) or inflating the airbags (fall catching). When trying to reach the desired inflation pressure, small leaks formed in the plastic liner. The airbags still stabilized the user, but due to the lower pressure, the user slipped downwards onto the fork.

Overall, both the elderly persons and the caretakers were supportive of the concept, especially the omnidirectional drive base which made positioning easy. Elderly users attested that the robot assisted with balance and body support, and the robot was successfully able to lift the user when necessary (see Fig. 9). The difficulty of each use case, rated by an adult participant, decreased from an average of 3.17/5 to 1.83/5, as the robot allowed the participant to perform the tasks with less perceived exertion. Importantly, the control scheme and added padding facilitated safe interactions with the elderly users, with no bruising or other injuries.

## VII. Conclusion and Discussion

We have developed an eldercare robot for postural assistance, body-weight lifting, ambulation support, and fall catching, without the need for a caregiver or a harness. Compared to previous designs, the robot's linkage has a larger range of motion, more natural trajectory, and desirable force/speed characteristics. Our target user group (elders with imbalance or who require assistive devices) is likely larger than anticipated, because elders tend to be overconfident in their abilities, leading to a discrepancy between physical risk and perceived risk that results in many falls each year [15].

Future work involves implementing autonomous navigation and automated fall detection. Caregivers and elderly persons also expressed a desire for a multimodal user interface, with cues such as lights to indicate the robot's direction of movement. With further modifications, we hope to eventually deploy our system in homes and care facilities.

## Acknowledgments

This material is supported by the National Robotics Initiative Grant No. 2133075 and the NSF GRFP under Grant No. 2141064. Human subject tests were reviewed and approved by MIT under IRB number 2207000712.

## REFERENCES


[1] United Nations, "World Social Report 2023: Leaving No One Behind in an Ageing World," www.un.org/development/desa/dspd/wp-content/uploads/sites/22/2023/01/2023wsr-chapter1-.pdf (accessed August 22, 2024).

[2] M. Whitley, "How Much Do Nursing Homes Cost? A State-By-State Guide," A Place For Mom, www.aplaceformom.com/caregiver-resources/articles/nursing-homes-cost (accessed August 22, 2024).

[3] J. Laughlin, "Home services and nursing care struggle amid Mass. health workforce crisis, new survey shows," Boston Globe, www.bostonglobe.com/2024/06/07/metro/home-care-nursing-massachusetts-health-labor-workforce-shortage/ (accessed August 22, 2024).

[4] D. Hipp, "Aging In Place Statistics And Facts In 2024," Forbes, www.forbes.com/health/healthy-aging/aging-in-place-statistics/ (accessed August 22, 2024).

[5] R. Kakara, G. Bergen, E. Burns, M. Stevens, "Nonfatal and Fatal Falls Among Adults Aged $\geq$65 Years—United States, 2020–2021," MMWR Morbidity and Mortality Weekly Report, 2023;72:938–943, DOI: 10.15585/mmwr.mm7235a1.

[6] R. Bolli, P. Bonato and H. Harry Asada, "A Handle Robot for Providing Bodily Support to Elderly Persons," 2023 IEEE/RSJ International Conference on Intelligent Robots and Systems (IROS), Detroit, MI, USA, 2023, pp. 122-129, doi: 10.1109/IROS55552.2023.10341348.

[7] R. Bolli and H. H. Asada, "Enhancing Elderly Mobility: A Sturdy, Two-Body Robot for Handlebar Placement in Any Location," in IEEE Robotics and Automation Letters, vol. 9, no. 3, pp. 2654-2661, March 2024, doi: 10.1109/LRA.2024.3359549.

[8] M. Toshiharu et al., "The strong robot with the gentle touch," RIKEN, www.riken.jp/en/news_pubs/research_news/pr/2015/20150223_2/ (accessed August 22, 2024).

[9] K. Barhydt and H. H. Asada, "A High-Strength, Highly-Flexible Robotic Strap for Harnessing, Lifting, and Transferring Humans," in IEEE Robotics and Automation Letters, vol. 8, no. 4, pp. 2110-2117, April 2023, doi: 10.1109/LRA.2023.3246389.

[10] D. Ding et al., "ReRobo Walker: Robotic Walker with Fall Detection and Active Safety," 2023 IEEE 18th Conference on Industrial Electronics and Applications (ICIEA), Ningbo, China, 2023, pp. 1562-1567, doi: 10.1109/ICIEA58696.2023.10241845.

[11] Panasonic Corporation, "Panasonic Launches New Services Using Walk Training Robot for Care Facilities," news.panasonic.com/global/press/en210427-4 (accessed August 22, 2024).

[12] S-AIRBAG, "S-AIRBAG Intelligent Vest S20", S-AIRBAG Official Online Store, sairbagpro.com/products/intelligent-airbag-protective-clothing-s32-b (accessed August 22, 2024).

[13] L. Li, M. J. Foo, J. Chen, et al., "Mobile Robotic Balance Assistant (MRBA): a gait assistive and fall intervention robot for daily living," J NeuroEngineering Rehabil 20, 29 (2023), doi.org/10.1186/s12984-023-01149-0.

[14] G. Iolascon et al., "The role of assistive devices in frail elderly people with fragility fractures: a narrative review," International Journal of Bone Fragility, 2021, doi: 10.57582/IJBF.210102.053.

[15] S. Stansfield, B. Schelhaas, N. Hogan, & M. Yang, "Understanding the User Perception Gap: Older Adults and Sit-to-Stand Assistance," Proceedings of the ASME 2023 International Design Engineering Technical Conferences and Computers and Information in Engineering Conference, Volume 6: 35th International Conference on Design Theory and Methodology (DTM), Boston, Massachusetts, USA, August 20–23, 2023.

[16] N. Gell et al., "Mobility device use in older adults and incidence of falls and worry about falling: findings from the 2011-2012 national health and aging trends study," J American Geriatrics Society, 2015.

[17] P. A. Desai and R. Mullerpatan, "Difficulties encountered in testing, scoring, and interpreting balance performance in older adults using clinical evaluation tools: a cross-sectional study," MGM Journal of Medical Sciences, 2023, doi: 10.4103/mgmj.mgmj_214_23.

[18] Massachusetts State Board of Building Regulations and Standards, "Special Detailed Requirements Based on Use and Occupancy - Means of egress," 780 CMR MA Code of Regs 408.3, regulations.justia.com/states/massachusetts/780-cmr/chapter-4/section-408/subsection-408-3/ (accessed August 23, 2024).

[19] D. Biman et al., "Isometric pull-push strengths in workspace: 1. Strength profiles," Int. J of Occupational Safety and Ergonomics, 2004.

[20] The Engineering ToolBox, "Typical Floor Loads: Uniformly and concentrated floor loads," engineeringtoolbox.com/floor-loads-uniformly-concentrated-d_2200.html (accessed September 9, 2024).

[21] I. Bytyçi, M. Henein, "Stride Length Predicts Adverse Clinical Events in Older Adults: A Systematic Review and Meta-Analysis," J Clin Med. 2021 Jun 17;10(12):2670, doi: 10.3390/jcm10122670.

[22] C. D. Fryar et al., "Mean body weight, height, waist circumference, and body mass index among adults: United States, 1999–2000 through 2015–2016," 2018 National Health Statistics Reports, no 122, Hyattsville, MD: National Center for Health Statistics.

[23] H. Jeong, A. Guo, T. Wang, M. Jun and Y. Ohno, "Development of Four-Bar Linkage Mechanism on Chair System for Assisting Sit-to-Stand Movement," 2019 IEEE 4th International Conference on Advanced Robotics and Mechatronics (ICARM), Toyonaka, Japan, 2019, pp. 303-308, doi: 10.1109/ICARM.2019.8833922.

[24] A. Mercader, M. Biersack, Y. Sun and T. C. Lueth, "A Mechanical Bed for Elderly Care to Assist while Standing, Sitting and Lying," 2019 IEEE International Conference on Robotics and Biomimetics (ROBIO), Dali, China, 2019, pp. 965-970, doi: 10.1109/ROBIO49542.2019.8961850.

[25] E. Ballesteros, S. -Y. Lee, K. C. Carpenter and H. Harry Asada, "Supernumerary Robotic Limbs to Support Post-Fall Recoveries for Astronauts," 2024 IEEE International Conference on Robotics and Automation (ICRA), Yokohama, Japan, 2024, pp. 2324-2331, doi: 10.1109/ICRA57147.2024.10610849.

[26] M. Sadeghi et al., "Trajectory of human movement during sit to stand: a new modeling approach based on movement decomposition and multi-phase cost function," Exp Brain Res., 2013, doi: 10.1007/s00221-013-3606-1.

[27] H. Wang et al., "Sit-to-Stand (STS) Movement Analysis of the Center of Gravity for Human–Robot Interaction," Front. Neurorobot, 2022, doi: 10.3389/fnbot.2022.863722.

[28] A. Dutra, "Driving Colson Wheels," Chief Delphi Forum, chiefdelphi.com/t/driving-colson-wheels/107415 (accessed August 28, 2024).

[29] M. Wada and S. Mori, "Holonomic and omnidirectional vehicle with conventional tires," Proceedings of IEEE International Conference on Robotics and Automation, Minneapolis, MN, USA, 1996, pp. 3671-3676 vol.4, doi: 10.1109/ROBOT.1996.509272.

[30] W. J. Choi, J. M. Wakeling and S. N. Robinovitch, "Kinematic analysis of video-captured falls experienced by older adults in long-term care", J. Biomech., vol. 48, no. 6, pp. 911-920, Apr. 2015.

[31] E. A. Kamienski, P. Bonato and H. H. Asada, "Time-Critical Fall Prediction Based on Lipschitz Data Analysis and Design of a Reconfigurable Walker for Preventing Fall Injuries," in IEEE Access, vol. 12, pp. 1822-1838, 2024, doi: 10.1109/ACCESS.2023.3347263.

[32] H. Black et al., "On the relationships between applied force, photography technique, and the quantification of bruise appearance," Forensic Science International, 2019, doi: 10.1016/j.forsciint.2019.109998.

[33] M. Zhang and A. F. Mak, "In vivo friction properties of human skin," Prosthet Orthot Int., 1999, doi: 10.3109/03093649909071625.